AJNR

STIR MR Imaging of the Orbit

Scott W. Atlas, Robert I. Grossman, David B. Hackney, Herbert I. Goldberg, Larissa T. Bilaniuk and Robert A. Zimmerman

AJNR Am J Neuroradiol 1988, 9 (5) 969-974
http://www.ajnr.org/content/9/5/969

STIR MR Imaging of the Orbit

Scott W. Atlas[1]
Robert I. Grossman
David B. Hackney
Herbert I. Goldberg
Larissa T. Bilaniuk
Robert A. Zimmerman

Fifteen patients with CT-documented orbital lesions were evaluated with MR imaging at 1.5 T with both conventional spin-echo (SE) and short inversion time inversion recovery (STIR) sequences. Fat signal was reliably nulled at inversion times of approximately 120–200 msec in all cases, thereby allowing clear detection of all retrobulbar lesions and normal structures on STIR images as markedly hyperintense relative to fat. All lesions were also clearly depicted on SE images; in fact, short repetition time/short echo time SE sequences were at least as useful as STIR images for illustrating anatomic structures and mass lesions, and in a much shorter scanning time. Separation of optic nerve from perioptic subarachnoid space was clear on SE images, but often difficult or impossible on STIR images owing to the relatively high intensity of normal optic nerves on STIR images. The synergism of relaxation prolongation with STIR actually resulted in loss of information, as any ability to separate the effects of T1 from T2 on signal intensity was impossible when STIR was the sole pulse sequence.

We believe that more information is obtained with standard SE sequences than with STIR sequences, and therefore SE remains the method of choice for orbital MR imaging.

Orbital lesions have been evaluated by many investigators with spin-echo (SE) MR imaging (1–9]; and with the more recent implementation of high-resolution surface-coil techniques [10, 11], significant advances have been made in MR imaging of the orbit. The orbit is somewhat unique in neuroradiology, in that the background stroma in this area is composed mainly of fat, which has a characteristic appearance on SE images. It has been proposed that short inversion time inversion recovery (STIR) would be useful in evaluating orbital disease [12, 13], since one can selectively suppress signal from a tissue (such as fat) based on its T1 by choosing the appropriate inversion time (TI) with this inversion recovery (IR) technique [14] and thereby highlight retrobulbar lesions, the vast majority of which are mainly water-containing. Furthermore, prolongation of T1 and T2, relaxation behavior characteristic of most diseases, is synergistic with STIR. These relaxation characteristics oppose each other in their contribution to signal intensity in SE imaging [15]. We evaluated the usefulness of STIR MR in depicting orbital disease in 15 patients and compared these images with SE images in these cases.

Subjects and Methods

Fifteen patients, ranging in age from 11 weeks to 66 years, with orbital lesions documented by CT were evaluated with MR imaging on a 1.5-T system.* All patients underwent both SE and STIR imaging, and images were obtained in the same plane in each patient with these techniques. SE sequences were performed with both short repetition time (TR)/short echo time (TE) sequences, 600/20/1 (TR/TE/excitations), and long TR/multiecho TE sequences, 2500/20–30, 80/2. STIR sequences used TRs of 800–2500 msec and TIs of 120–200 msec. The TIs were selected for the purpose of suppressing signal from fat [13]. All images were displayed with magnitude reconstruction. The appearance of lesions, as well as normal retrobulbar structures, was compared by using these two techniques.

* General Electric Medical Systems, Milwaukee, WI.

This article appears in the September/October 1988 issue of *AJNR* and the November 1988 issue of *AJR*.

Received September 16, 1987; accepted after revision February 18, 1988.

Presented at the annual meeting of the American Society of Neuroradiology, New York City, May 1987.

[1] All authors: Department of Radiology, Hospital of the University of Pennsylvania, 3400 Spruce St., Philadelphia, PA 19104. Address reprint requests to S. W. Atlas.

***AJNR* 9:969–974, September/October 1988**
0195–6108/88/0905–0969

The signal intensity (SI) within a pixel acquired with IR can be determined from the equation [15],

$$SI = k \times N(H)\,(e^{-TE/T2})[1 - 2\,(e^{-TI/T1}) + e^{-TR/T1}], \quad (1)$$

where k = a constant expressing system gain, N(H) is the mobile proton density, and T1 and T2 are the longitudinal and transverse relaxation times, respectively. The TI at the "null point" (i.e., the value of TI for which SI equals zero for the tissue with a specific T1) is given by the equation [15],

$$TI_{null} = -T1 \times \ln[\tfrac{1}{2}(1 + e^{-TR/T1})]. \quad (2)$$

For $TR \gg T1$, TI_{null} is given by the approximation [13],

$$TI_{null} = T1 \times \ln 2. \quad (3)$$

With magnitude image reconstruction techniques (when TI is selected for the purpose of nulling signal from fat), tissues that have recovered longitudinal magnetization either more or less than fat will have a positive signal intensity (and fat will demonstrate very low signal). The TI_{null} for fat was determined either from approximation from equation 2, based on a T1 of 200–250 msec for orbital fat [16] or from direct observation of fat signal peak nulling on the signal profile obtained during the prescan with changes in TI [17].

Short TR scans were acquired in 2 min 51 sec. Long TR scans were obtained in 10 min 30 sec. STIR scans were obtained in times ranging from 3 min 40 sec to 10 min 30 sec, depending on the TR.

Results

All lesions were clearly delineated by both SE and STIR techniques. Short TR/TE SE images demonstrated all lesions, as well as normal retrobulbar anatomy, clearly depicting them against a high-intensity background of retrobulbar fat (Figs. 1–3). Clear definition of perioptic CSF separate from the optic nerve was usually possible with both short TR/TE and long TR/TE scans (Figs. 1, 2, and 4). On Long TR/TE images, lesions were portrayed against the background of low-intensity orbital fat (Figs. 1–4). Normal extraocular muscles were only minimally hyperintense or isointense relative to fat on this sequence. On SE sequences, the well-known misregistration bands of high intensity and low intensity at fat-water interfaces [18] were noted along the frequency-encoding axis (Fig. 1). These artifacts, although often fairly prominent on SE images, were not problematic in any case.

Fat signal was consistently suppressed on STIR imaging at TIs of 120–200 msec in these 15 patients, thereby depicting all other normal retrobulbar structures as relatively hyperintense. Changes in TR alter signal intensities in STIR, since TI_{null} is different if TR is not sufficiently long (equation 2). Increased TR also increases overall signal. Varying TE also changes signal intensities somewhat, since a longer TE adds contrast on the basis of T2 differences (i.e., lesions with long T2 will have a higher signal intensity with a long TE). Relatively small changes in TI resulted in markedly different contrast relationships (Fig. 5). Therefore, on STIR images, extraocular muscles and optic nerves were markedly hyperintense relative to fat. It was usually difficult and often virtually impossible to separate optic nerve from surrounding CSF because of the high intensity of normal optic nerve (Figs. 1–4). The high-intensity band at one edge of fat-water interfaces from chemical-shift misregistration [18] was eliminated when signal from fat was nulled (Fig. 1). A region of signal void was identifiable on STIR images at all fat-water interfaces (Figs. 3C, 4B, and

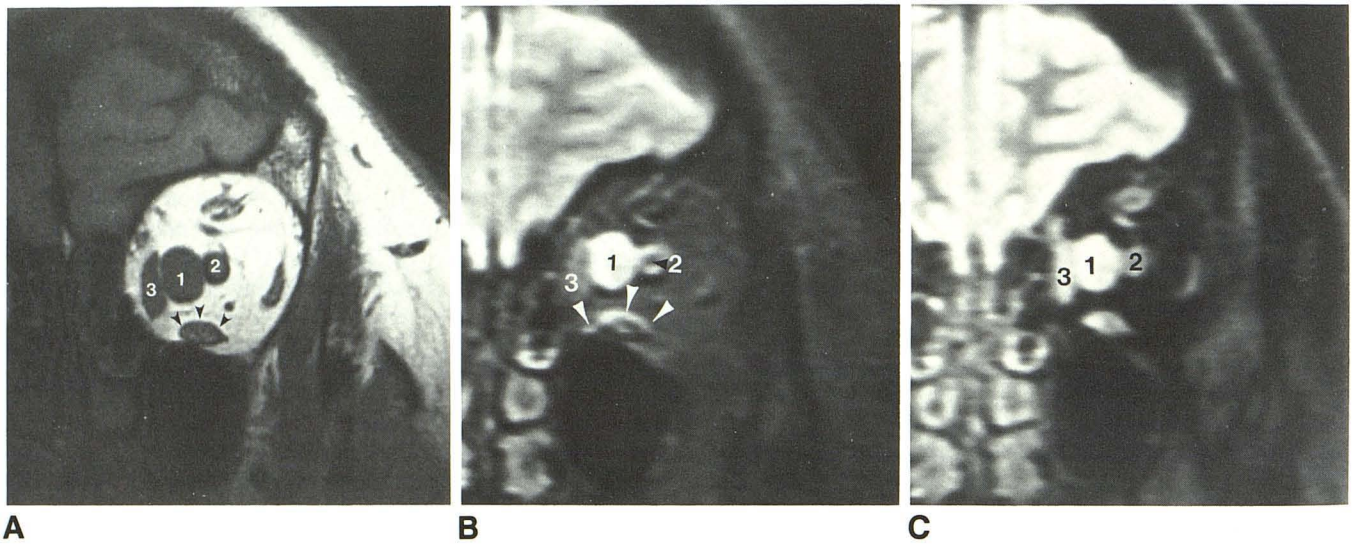

Fig. 1.—Intraconal cavernous hemangioma.
***A*, Coronal SE image, 600/20.**
***B*, Coronal SE image, 2500/80.**
***C*, Coronal STIR image, 2500/140/20.**
Well-circumscribed mass (1) is well delineated between optic nerve (2) and medial rectus muscle (3) on all sequences. Mass is isointense relative to muscle on short TR/TE (*A*) and markedly hyperintense on long TR/TE (*B*) images. Mass is hyperintense relative to fat, but approximately isointense relative to muscle, on STIR image (*C*). Note chemical-shift artifacts (*arrowheads*) on SE images (*A* and *B*), which are absent on STIR image (*C*). Also, relative hyperintensity of optic nerve (2) on STIR image is not easily distinguishable from perioptic CSF.

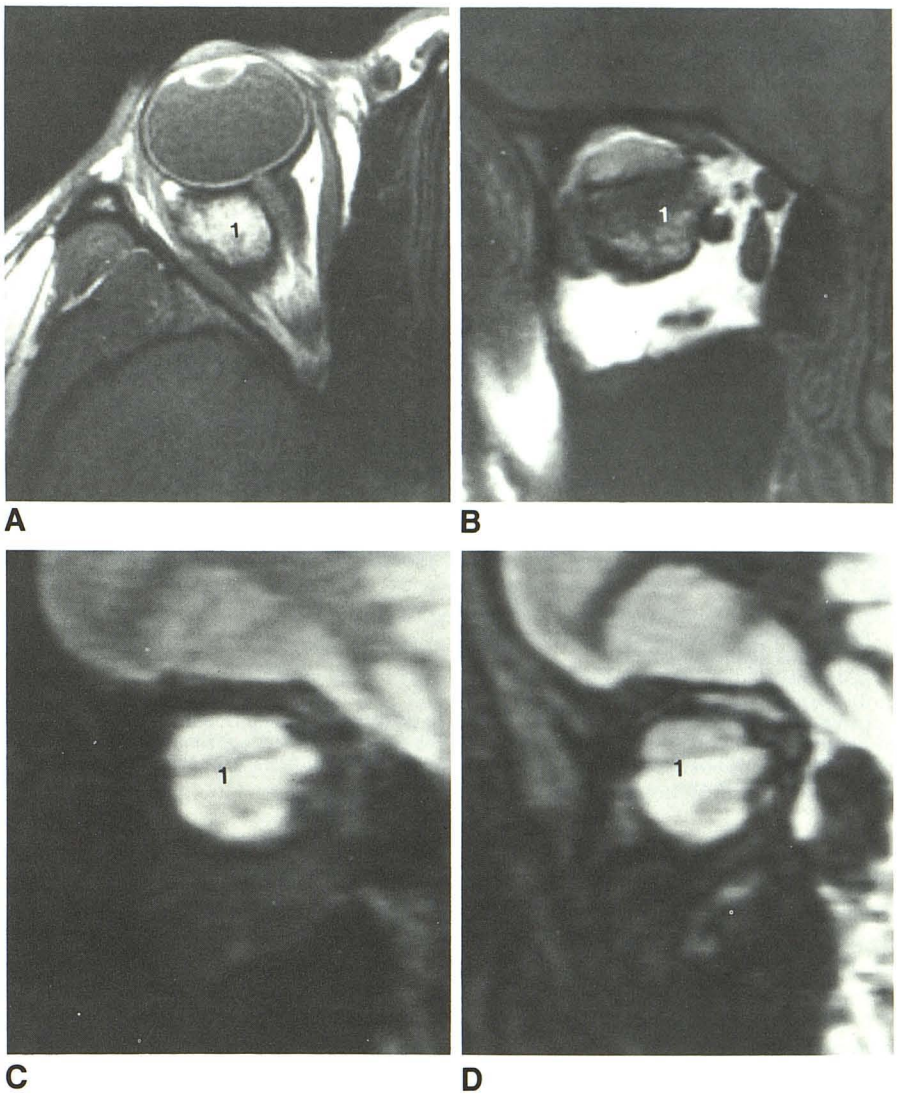

Fig. 2.—Intraconal, partially thrombosed cavernous hemangioma.
***A*, Axial SE image, 600/20.**
***B*, Coronal SE image, 600/20.**
***C*, Coronal SE image, 2500/80.**
***D*, Coronal STIR image, 2500/200/25.**
Marked inhomogeneity in mass (1) on all sequences is consistent with partial thrombosis of cavernous hemangioma, which deviates optic nerve medially. Note clear separation of optic nerve from perioptic CSF on short TR/TE images (*A* and *B*) but not on STIR image (*D*). In this case, long TR/TE image (*C*) does not clearly distinguish optic nerve from perioptic CSF.

5) [19]. All lesions were markedly hyperintense relative to fat on STIR sequences (Figs. 1–4).

Intralesional heterogeneity was depicted on all SE sequences as well as on STIR when present in any sequence (Fig. 2).

Discussion

IR imaging has been applied to various areas of the body for obtaining images with high contrast, the degree of which is mainly dependent on the TI and its relationship to the T1 of the tissue of interest [14, 15]. A unique characteristic of IR sequences is the phenomenon of signal nulling. This phenomenon is due to partial recovery of longitudinal magnetization after the initial 180° RF inverting pulse just to the "crossover" point [15], so that the subsequent 90° pulse eliminates all magnetization in the transverse plane just before signal detection. This results in the depiction of all tissue with that particular T1 as very low signal [14, 15]. The null-pont TI (TI_{null}) is based on the T1 of the tissue from which one is interested in nulling the signal (Fig. 6). TI_{null} can be determined from the signal-intensity equation (equation 1) for IR [15]. If one considers situations in which TR is $\gg$ T1 than the equation simplifies to equation 3.

Therefore, one can approximate TI_{null} by multiplying $0.69 \times$ T1. (Note that the TI_{null} will vary with applied field strength, since T1 changes with field-strength changes.) A more accurate and individualized assessment of TI_{null} can also be obtained by direct observation of the signal profile obtained from prescanning, whereby the (major) fat peak is separable from the water peak (due to the 3.5-ppm difference in resonant frequencies of fat and water protons) [18, 20]. By varying TI, one can visualize suppression of the fat peak, thereby obtaining the TI_{null} for each patient individually [17]. This method of prescanning can be performed in about 2 min. STIR sequences theoretically can be used to highlight all lesions residing in a tissue with a T1 significantly different from the T1 of those lesions simply by selecting TI to concur with the quantity, $0.69 \times$ T1 of the background normal tissue. This has been applied with some success to detecting intrahepatic

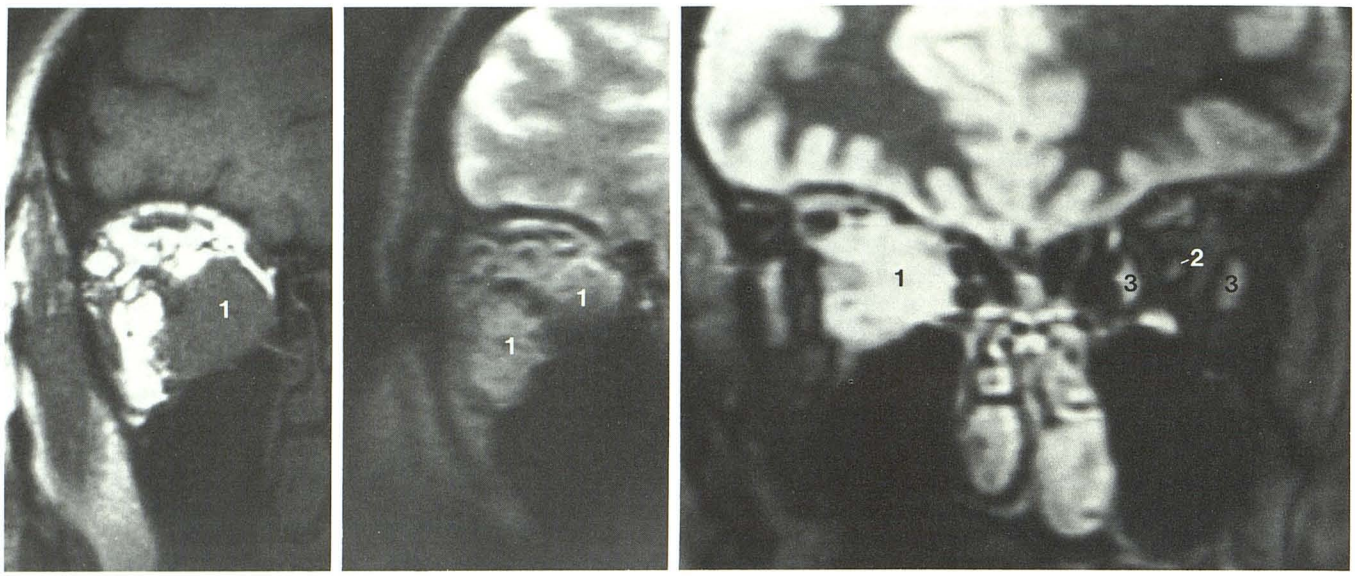

Fig. 3.—Inflammatory orbital pseudotumor.
A, Coronal SE image, 600/20.
B, Coronal SE image, 2500/80.
C, Coronal STIR image, 2500/200/20.
Large retrobulbar mass (1) is isointense relative to fat on long TR/long TE image (*B*), characteristic of benign inflammatory pseudotumor as opposed to malignant lesions. STIR image (*C*) depicts mass, however, as markedly hyperintense, indistinguishable from malignant lesions such as lymphoma. Also note again hyperintense optic nerve (2) and extraocular muscles (3) on STIR image (*C*). Boundary artifact of hypointensity is located at all fat-water interfaces on STIR image.

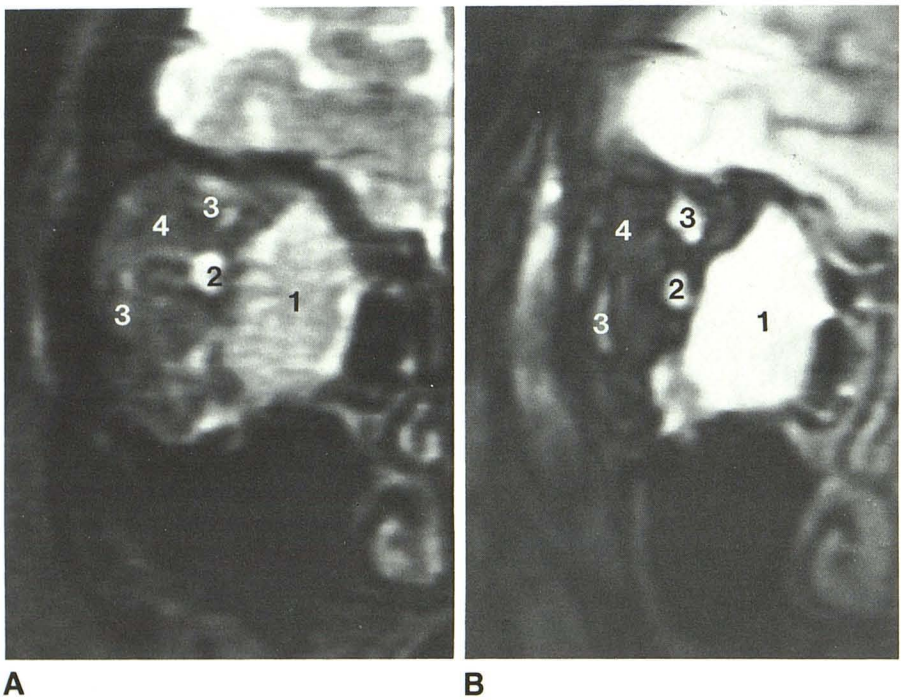

Fig. 4.—Orbital lymphoma.
A, Coronal SE image, 2500/80.
B, Coronal STIR image, 2500/150/20.
Large mass (1) in medial aspect of orbit is hyperintense on both long TR/TE SE (*A*) and STIR (*B*) sequences. Note marked contrast between hyperintense optic nerve (2) and hyperintense extraocular muscles (3) vs markedly hypointense fat (4) on STIR image.

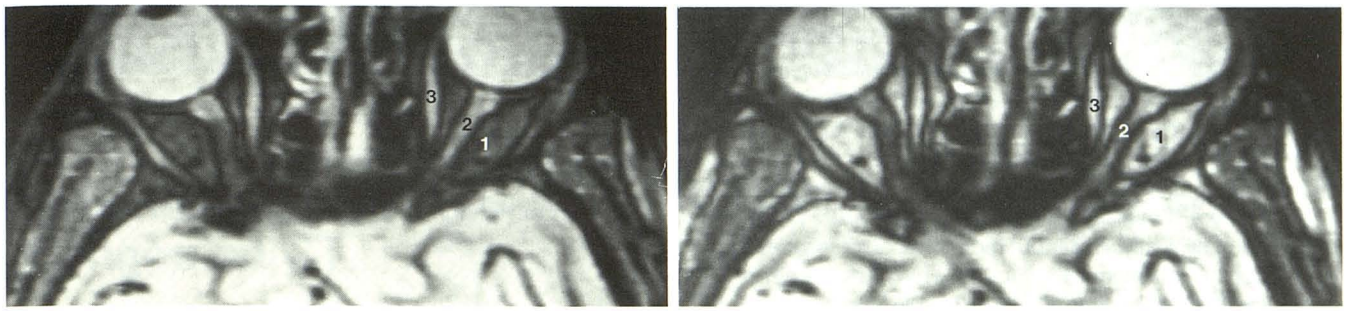

A B

Fig. 5.—Effect on contrast of changes in TI.
***A*, Axial STIR image, 2500/200/20.**
***B*, Axial STIR image, 2500/250/20.**
Note total inversion of contrast relationships in retrobulbar structures between fat (1) and water-containing structures with 50-msec change in TI. When TI is selected so that signal from fat is nulled (*A*), all retrobulbar structures, including optic nerve (2) and extraocular muscles (3), are markedly hyperintense. It is impossible to separate perioptic CSF from optic nerve on this image. Also note marked hypointensity (boundary artifact) at all fat-water interfaces on both STIR sequences.

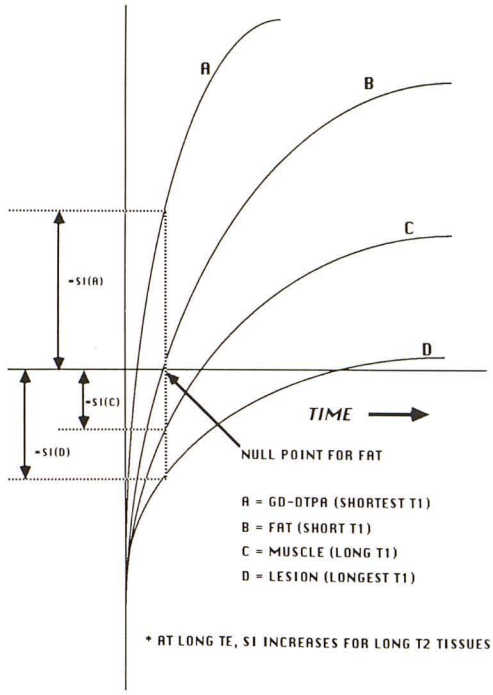

Fig. 6.—Signal intensity (SI) vs T1 at null point for fat. Note that rate of recovery of longitudinal magnetization (i.e., T1), relative to TI, determines signal intensity as compared with nulled tissue (fat). In addition, as TE is increased, tissues with longer T2 will have higher signal intensity. Therefore, lesions with long T1 and long T2 will have increased intensity because of both these factors.

lesions [14]. It has been suggested that STIR might be very useful in the orbits [12, 13], since most of the retrobulbar compartment is occupied by fat, which has a T1 significantly different from the T1 of other (water-containing) orbital structures and from the expected T1 of the vast majority of (water-containing) orbital lesions. Furthermore, a relatively long TE can also be selected with STIR, so that prolongation of T1 and prolongation of T2 both cause an increase in signal intensity. This synergistic effect of T1 and T2 prolongation is opposite to the effect on signal intensity of increased T1 and T2 in SE sequences; that is, an increase in T1 reduces signal intensity and an increase in T2 increases signal intensity on SE imaging [15]. Since the great majority of lesions exhibit long T1 and long T2, theoretically STIR would be more sensitive to subtle changes in relaxation parameters, which, at least in theory, might not be detected easily on SE images. Increases in spin density further augment signal intensity in both STIR and SE imaging.

In our series, STIR sequences did indeed depict lesions with marked conspicuity against a background of very-low-intensity orbital fat (Figs. 1–4). In fact, all retrobulbar structures, including extraocular muscles and the optic nerve/sheath complex, were markedly hyperintense on STIR images. This allowed superb delineation of anatomic relationships behind the globe, and when comparing the long TR/long TE SE image with the STIR image (on both images, fat is low-intensity), there was no question that STIR depicted extraocular muscles and optic nerves with greater contrast than did the long TR/TE SE images (Figs. 1–4). However, short TR/TE SE images also allowed superb anatomic delineation of retrobulbar structures, differing from STIR only in that the fat background was of high rather than low intensity. Furthermore, separation of optic nerve from the surrounding CSF was usually accomplished easily with both short and long TR/TE SE images (Figs. 1, 2, and 4). In our experience, this separation was difficult on STIR images, since the normal optic nerve is relatively hyperintense (Figs. 1–5) when fat signal is suppressed.

All lesions were markedly hyperintense on STIR sequences. Although in theory the synergism of prolonged T1 and T2 might be beneficial for detecting subtle retrobulbar changes, no lesion in our series seen on STIR was not detectable on short TR/TE, long TR/short TE, or long TR/long TE SE images. Other authors, however, have noted the usefulness of STIR for documenting optic neuritis [13]. In addition, separation of intrinsic relaxation behavior characteristics, attainable (to a certain extent) from analysis of the three SE images, was virtually impossible from an analysis of STIR images,

since prolonged T1, prolonged T2, and increased spin density all increase signal intensity on STIR. This is particularly disturbing in the evaluation of orbital pseudotumor, which has been reported to demonstrate relatively characteristic signal-intensity patterns on SE images [21], probably related to the highly fibrous nature of this entity. These lesions are usually isointense or only minimally hyperintense relative to fat on long TR/long TE SE images (Fig. 3), in contrast to the appearance of clinically similar but more ominous diseases, such as retrobulbar malignancies (Fig. 4), which are usually markedly hyperintense on long TR/long TE SE images [21]. STIR depicts both types of disease as markedly hyperintense, reducing any potential specificity for MR imaging in distinguishing these lesions. Furthermore, contrast relationships that use STIR sequences are highly dependent on accurate flip angles, since errors in flip angle would alter the null point and would dramatically change relative signal intensities.

One side benefit to suppressing signal from orbital fat is the elimination of the high-intensity band perpendicular to the frequency-encoding axis seen on SE images at fat-water interfaces due to misregistration (Fig. 1) [18]. Practically speaking, however, this chemical-shift misregistration artifact is now well known to all those who interpret SE images and is rarely a problem in diagnosis. Other, more rapid methods have been proposed to eliminate possible confusion from this artifact in orbital imaging [22, 23]. In fact, another artifact is present on STIR images at fat-water interfaces, consisting of a rim of signal void (Figs. 3C, 4B, and 5). This can be ascribed to intravoxel signal cancellation when longitudinal magnetization of different materials are approximately equal in magnitude but opposite in direction (i.e., they are 180° out of phase). In this case, voxels that derive signal contributions equally from fat and water protons (such as the situation at fat-water interfaces) have a recovered longitudinal magnetization that averages to zero. This situation, in fact, is the same as if the T1 of the voxel corresponded to the null point. This has been termed the "opposed magnetization artifact," which depends on the difference in T1s between tissues rather than on relative chemical-shift differences [19].

In conclusion, STIR imaging can be performed to successfully suppress signal intensity from orbital fat and thereby provide high-contrast images of the orbit. These images allow excellent anatomic delineation of normal structures as well as retrobulbar mass lesions. All lesions in our series were depicted as markedly hyperintense on STIR images. However, short TR/TE SE sequences were equally useful in illustrating anatomic structures and mass lesions, and in a much shorter scanning time. This decrease in scanning time allows high-resolution surface-coil imaging to be performed with less interference from motion artifacts, a frequent problem in orbital MR imaging. Furthermore, separation of optic nerve from perioptic subarachnoid CSF was clear on SE images, but often difficult or impossible when STIR was the sole pulse sequence. Although the high intensity of chemical-shift artifacts was virtually eliminated with STIR, these artifacts are well known and easily recognizable on SE images. Therefore, despite the high-contrast images of the orbit produced by STIR, which allows excellent anatomic delineation of normal structures and mass lesions, we believe that more information is obtained with standard SE sequences, and therefore SE remains the method of choice for orbital MR imaging.

ACKNOWLEDGMENT

We thank Kara R. Reynolds for assistance in manuscript preparation.

REFERENCES

1. Hawkes RC, Holland GN, Moore WS, Rizk S, Worthington BS, Kean M. NMR imaging in the evaluation of orbital tumors. *AJNR* **1983**;4:254–256
2. Edwards JH, Hyman RA, Vacirca SJ, et al. 0.6 T magnetic resonance imaging of the orbit. *AJNR* **1985**;6:253–258
3. Daniels DL, Herfkens RJ, Gager WE, et al. Magnetic resonance imaging of the optic nerves and chiasm. *Radiology* **1984**;152:79–83
4. Hans JS, Benson JE, Bonstelle CT, Alfidi RJ, Kaufman B, Levin M. Magnetic resonance imaging of the orbit: a preliminary experience. *Radiology* **1984**;150:755–759
5. Bilaniuk LT, Schenck JF, Zimmerman RA, et al. Ocular and orbital lesions: surface coil MR imaging. *Radiology* **1985**;156:669–674
6. Sobel DR, Kelly WM, Kjos BO, Char D, Brandt-Zawadzki M, Norman D. MR imaging of orbital and ocular disease. *AJNR* **1985**;6:259–264
7. Sullivan JA, Harms SE. Surface-coil MR imaging of orbital neoplasms. *AJNR* **1986**;7:29–34
8. Mafee MF, Peyman GA, Grisolano JM, et al. Malignant uveal melanoma and simulating lesions: MR imaging evaluation. *Radiology* **1986**;160:773–780
9. Atlas SW, Bilaniuk LT, Zimmerman RA, Hackney DB, Goldberg HI, Grossman RI. Orbit: initial experience with surface coil spin-echo MR imaging at 1.5 T. *Radiology* **1987**;164:501–509
10. Schenck JF, Hart HR Jr, Foster TH, et al. Improved MR imaging of the orbit at 1.5T with surface coils. *AJNR* **1985**;6:193–196
11. Schenck JF, Hart HR, Foster TH, Edelstein WA, Hussain MA. High resolution magnetic resonance imaging using surface coils. In: Kressel HY, ed. *Magnetic resonance annual 1986*. New York: Raven, **1986**:123–160
12. Smith FW, Parek HS, Forrester J, Redpath TW. MR imaging of the orbit and eye using inversion recovery sequences. *Radiology* **1986**;161(p):286
13. Johnson G, Miller DM, MacManus D, et al. STIR sequences in NMR imaging of the optic nerve. *Neuroradiology* **1987**;29:238–245
14. Bydder GM, Young IR. MR imaging: clinical use of the inversion recovery sequence. *J Comput Assist Tomogr* **1985**;8:585–587
15. Wehrli FW, MacFall JR, Glover GH, et al. Dependence of nuclear magnetic resonance (NMR) image contrast on intrinsic and pulse sequence timing parameters. *Radiology* **1985**;157:573
16. Bottomley PA, Foster TH, Arsinger RE, Pfeifer LM. A review of normal tissue hydrogen NMR relaxation times and relaxation mechanisms from 1-100 MHz: dependence on tissue type, NMR frequency, temperature, species, excision, and age. *Med Phys* **1984**;11:425–448
17. Newman R. *Operator's pulse sequence data notes.* Milwaukee: General Electric, **1987**
18. Babcock EE, Brateman L, Weinreb JC, Horner SD, Nunnally RL. Edge artifacts in MR images: chemical shift effect. *J Comput Assist Tomogr* **1985**;9:252–257
19. Hearshen DO, Ellis JH, Carson PL, Shreve P, Aisen AM. Boundary effects from opposed magnetization artifact in IR images. *Radiology* **1986**;160:543–547
20. Dixon WT. Simple proton spectroscopic imaging. *Radiology* **1984**;153:189–194
21. Atlas SW, Grossman RI, Savino PJ, et al. Surface coil MR of orbital pseudotumor. *AJNR* **1987**;8:141–146
22. Daniels DL, Kneeland JB, Shimakawa A, et al. MR imaging of the optic nerve and sheath: correcting the chemical shift misregistration effect. *AJNR* **1986**;7:249–253
23. Atlas SW, Grossman RI, Axel L, et al. Orbital lesions: proton spectroscopic phase-dependent contrast MR imaging. *Radiology* **1987**;164:510–514